Podocyte injury-driven intracapillary plasminogen activator inhibitor type 1 accelerates podocyte loss via uPAR-mediated β_1-integrin endocytosis

Namiko Kobayashi,[1] Toshiharu Ueno,[1] Kumi Ohashi,[1] Hanako Yamashita,[1] Yukina Takahashi,[1] Kazuo Sakamoto,[1] Shun Manabe,[1] Satoshi Hara,[1] Yasutoshi Takashima,[1] Takashi Dan,[2] Ira Pastan,[3] Toshio Miyata,[2] Hidetake Kurihara,[4] Taiji Matsusaka,[5] Jochen Reiser,[6] and Michio Nagata[1]

[1]*Department of Pathology, Graduate School of Comprehensive Human Sciences, University of Tsukuba, Ibaraki, Japan;*
[2]*Center for Translational and Advanced Research, Tohoku University Graduate School of Medicine, Sendai, Miyagi, Japan;*
[3]*Laboratory of Molecular Biology, Center for Cancer Research, National Cancer Institute, National Institutes of Health, Bethesda, Maryland;* [4]*Department of Anatomy, Juntendo University School of Medicine, Bunkyo, Tokyo, Japan;* [5]*Department of Internal Medicine, Institute of Medical Science, Tokai University School of Medicine, Isehara, Kanagawa, Japan; and* [6]*Department of Medicine, Rush University, Chicago, Illinois*

Kobayashi N, Ueno T, Ohashi K, Yamashita H, Takahashi Y, Sakamoto K, Manabe S, Hara S, Takashima Y, Dan T, Pastan I, Miyata T, Kurihara H, Matsusaka T, Reiser J, Nagata M. Podocyte injury-driven intracapillary plasminogen activator inhibitor type 1 accelerates podocyte loss via uPAR-mediated β_1-integrin endocytosis. *Am J Physiol Renal Physiol* 308: F614–F626, 2015. First published January 13, 2015; doi:10.1152/ajprenal.00616.2014.— Podocyte-endothelial cell cross-talk is paramount for maintaining the filtration barrier. The present study investigated the endothelial response to podocyte injury and its subsequent role in glomerulosclerosis using the podocyte-specific injury model of NEP25/LMB2 mice. NEP25/LMB2 mice showed proteinuria and local podocyte loss accompanied by thrombotic microangiopathy on *day 8*. Mice showed an increase of glomerular plasminogen activator inhibitor type 1 (PAI-1) mRNA and aberrant endothelial PAI-1 protein already on *day 1*, before thrombosis and proteinuria. A PAI-1-specific inhibitor reduced proteinuria and thrombosis and preserved podocyte numbers in NEP25/LMB2 mice by stabilization of β_1-integrin translocation. Heparin loading significantly reduced thrombotic formation, whereas proteinuria and podocyte numbers were unchanged. Immortalized podocytes treated with PAI-1 and the urokinase plasminogen activator (uPA) complex caused significant cell detachment, whereas podocytes treated with PAI-1 or uPA alone or with the PAI-1/uPA complex pretreated with an anti-uPA receptor (uPAR) antibody failed to cause detachment. Confocal microscopy and cell surface biotinylation experiments showed that internalized β_1-integrin was found together with uPAR in endocytotic vesicles. The administration of PAI-1 inhibitor or uPAR-blocking antibody protected cultured podocytes from cell detachment. In conclusion, PAI-1/uPA complex-mediated uPAR-dependent podocyte β_1-integrin endocytosis represents a novel mechanism of glomerular injury leading to progressive podocytopenia. This aberrant cross-talk between podocytes and endothelial cells represents a feedforward injury response driving podocyte loss and progressive glomerulosclerosis.

podocyte; plasminogen activator inhibitor type 1; endocytosis; integrin; kidney; pathology

PODOCYTE INJURY and the subsequent cell loss promote glomerulosclerosis in various glomerular diseases (7, 8, 21, 43). However, there is limited information describing the detailed mechanism of podocyte injury-induced glomerulosclerosis. In the remnant kidney model, segmental podocyte loss was accompanied by synechiae formation to Bowman's capsule, leading to segmental sclerosis (27, 28). A more progressive podocyte loss model was followed by Notch1-mediated parietal epithelial cell migration leading to collapsing focal segmental glomerulosclerosis (FSGS); thus, podocyte loss triggers a maladaptive extracapillary response leading to sclerosis (39).

The glomerular filtration barrier is composed of podocytes, the glomerular basement membrane (GBM), and endothelial cells (8). Homeostatic regulation of filtration barrier function has been suggested to be maintained by cross-talk signaling between podocytes and endothelial cells. Electron microscopy showed a close association of endothelial cell abnormalities and overlying podocyte injury in various models of glomerulosclerosis, suggesting a causal relationship between these two cells (12, 22). Bevacizumab is an anti-VEGF antibody used in the treatment of cancer that occasionally causes glomerular thrombotic microangiopathy (TMA), and mice with podocyte-specific VEGF depletion have intracapillary lesions similar to TMA (12). These observations suggest that podocyte-derived VEGF preserves intracapillary homeostasis; however, the molecular basis of the intracapillary response to podocyte injury and its role in progressive glomerular damage has not been delineated. Blockade of endothelial VEGF transport in mice deficient in EH-domain containing 3/4 caused podocyte foot processes effacement (13). Shear stress in glomerular endothelial cells in vitro changed the actin arrangement in cocultured podocytes via ERK5-mediated vasodilator-stimulated phosphoprotein phosphorylation (36). Additionally, transient podocyturia and heavy proteinuria accompany pregnancy-induced hypertension, of which the pathophysiological base is severe endothelial cell injury (1). These findings suggest that podocyte injury triggers intracapillary-derived aberrant podocyte danger signals that underlie glomerular diseases.

Plasminogen activator inhibitor type 1 (PAI-1) is synthesized by several cell types and is known to inhibit fibrinolysis to stop bleeding by inactivating tissue plasminogen activator and urokinase plasminogen activator (uPA) (31, 44). Additionally, PAI-1 has several pleiotropic actions, including effects on cell survival, proliferation, motility, and mobility (9, 24). Notably, PAI-1 is not expressed in normal kidney glomeruli (10). Instead, PAI-1 is upregulated in glomeruli of patients with FSGS and membranous nephropathy, both of which are

podocyte diseases (14, 29, 45). PAI-1 interacts with the uPA receptor (uPAR), which is upregulated in podocytes undergoing injury, and the soluble form of uPAR can drive the onset of FSGS via interactions with the podocyte integrin system (41, 42). These findings suggest a novel action of glomerular PAI-1 on podocyte diseases.

The present study aimed to investigate the glomerular intracapillary response to primary podocyte injury and its role in disease progression using a transgenic murine model of podocyte-selective injury (26). Our results showed that aberrant intracapillary signals associated with podocyte injury accelerated podocyte loss due to local PAI-1/uPA complex formation, which mediated its effect through uPAR-dependent β_1-integrin endocytosis by podocytes. This suggests a novel mechanism for a vicious cycle of podocyte loss. Additionally, since PAI-1 inhibition ameliorates this exacerbated podocyte loss, our work suggests a novel therapeutic option for podocyte injury-driven glomerulosclerosis.

MATERIALS AND METHODS

Animal Experiments

We used well-established NEP25 mice treated with an immunotoxin (LMB2 NEP25/LMB2 mice) (26), a FSGS model driven by podocyte-specific injury. NEP25 mice with the C57BL/6J genetic background selectively express human CD25 on podocytes. Podocyte-specific injury was induced by human CD25-specific antibody (LMB2), as previously described (26, 39). The toxin was given once; it disappeared after 35 min and set in motion a cascade leading to podocyte depletion. Mice were treated humanely and housed in animal facilities with free access to food and water, according to protocols approved by the Institutional Animal Use and Care Committee of the University of Tsukuba (Registered No. 11-305).

Protocols

Protocol 1: microangiopathic assessment of podocyte injury in NEP25 mice injected with LMB2. NEP25 mice aged 12–18 wk ($n = 32$) were randomly divided into two groups: *1*) NEP25/LMB2 mice anesthetized with isoflurane and injected with LMB2 intravenously ($n = 26$, 4 ng/g body wt) on *day 0* and *2*) NEP25/PBS mice injected with PBS intravenously as controls ($n = 6$). The LMB2 dosages used in this experiment induces severe nephrosis and mice died at 2 wk, as previously described (26, 39). Our preliminary study showed no proteinuria in wild-type littermate mice treated with LMB2. Histopathology was conducted in both groups (with LMB2: $n = 6$ and with PBS: $n = 6$). Renal samples were obtained by biopsy (on *days −1* and *8*) and autopsy at death (on *day 12*). Proteinuria was measured on *days −1, 0, 5, 8*, and *12* after injection and estimated as the urinary protein-to-creatinine ratio. For real-time PCR, glomeruli were isolated from each animal, NEP/LMB2 mice on *days −1* ($n = 5$), *1* ($n = 5$), *8* ($n = 5$), and *12* ($n = 5$), and were statistically analyzed.

Protocol 2: effect of PAI-1 inhibition on NEP25 mice injected with LMB2. NEP25/LMB2 mice aged 12–18 wk ($n = 24$) were divided into two groups: *1*) PAI-1 inhibitor-treated NEP25/LMB2 mice (NEP25/LMB2 + PI) and *2*) vehicle-treated NEP25/LMB2 mice (NEP25/LMB2 + VH). NEP25/LMB2 + PI mice were administered the PAI-1 inhibitor TM5484 (10 μg/g body wt in 0.5% carboxymethyl cellulose sodium, $n = 13$) orally for 12 days. As the half-life of LMB2 is 35 min, the PAI-1 inhibitor was initially administered 2 h after LMB2 injection. NEP25/LMB2 + VH mice ($n = 11$) were administered vehicle orally for 12 days after LMB2 injection. The details of PAI-1 inhibitor are summarized below. Histology and real-time PCR were performed on biopsies from NEP25/LMB2 + PI ($n = 8$) and NEP25/LMB2+VH ($n = 6$) mice on *days −1* and *8* and on *day 12* at

death. Biopsy samples contained over 30 glomeruli in a single section. After LMB2 injection, 24-h urine samples were collected on *days −1, 0, 5, 8*, and *12*. Glomeruli were isolated from both groups ($n = 5$ mice/group) at death and used for real-time PCR.

The PAI-1 inhibitor TM5484 (molecular weight: 384.8 g/mol, clogP: 2.32) was designed based on structures of the PAI-1 inhibitor TM5007 (19). TM5007 was the initial compound identified virtually by structure-based drug design after undergoing a docking simulation that selected for compounds that fit within the cleft of PAI-1 (s3A in the human PAI-1 three-dimensional structure) and was accessible to insertion of the reactive center loop (18, 19). The design of TM5484 was processed by an extensive structural activity relationship study among >450 novel derivatives of TM5007 with comparatively low molecular weight (400–550 g/mol) without symmetrical structure (17). The inhibitory activity of TM5484 was shown in vitro by a chromogenic assay (IC$_{50}$: 3.56 μM), and its specificity was confirmed by demonstrating that it did not inhibit other serpins, such as antithrombin III and α_2-antiplasmin. A repeated dose toxicity study of TM5484 was assessed for 2 wk in five rats per gender per group, and no adverse effect level was concluded at 30 mg/kg. Regarding the reverse mutation Ames test, evaluation of TM5484 produced a negative result. The effect of TM5484 on human *ether-a-go-go*-related gene (hERG) electric current was investigated in human embryonic kidney-293 cells transfected with the hERG gene. TM5484 was found not to have an effect on hERG electric current at concentrations up to 10 μmol/l. We assessed the average bleeding time in NEP25/PBS mice by tail cut ($n = 3$). Average bleeding times after TM5484 treatment were 165 ± 39.7 s at preadministration, 375 ± 68.7 s at maximal time (2 h for TM5484, $P < 0.05$ vs. preadministration), and 341.7 ± 3.33 s at 24 h, which indicated the effects of TM5484 in the NEP25 mouse model.

Protocol 3: effect of heparin loading on NEP25/LMB2 mice. NEP25/LMB2 mice aged 12–18 wk ($n = 10$) were divided into two groups: *1*) NEP25/LMB2 mice treated with 25 units of heparin sodium (Fuji Pharma, Tokyo, Japan) through subcutaneous injection twice daily from *days −1* to *11* (NEP25/LMB2 + Hep; $n = 5$) and *2*) NEP25/LMB2 mice treated with PBS (NEP25/LMB2 + PBS; $n = 5$), which were considered controls. The anticoagulant effect of heparin was determined by the coagulation time, as revealed by a recalcification coagulation assay (16). The dosage of heparin sodium used was determined by keeping the coagulation time three times longer than that for control mice. Histology was performed on *day −1* by biopsy and on *day 12* at death. Proteinuria was estimated on *days 0, 5, 8*, and *12*. Number of Wilms tumor 1 (WT-1)-positive cells and thrombosis scores were estimated on *days −1* and *12*.

Staining and Morphological Analysis

Kidneys were fixed in 4% paraformaldehyde and embedded in paraffin. Parts of the kidney samples were incubated in graded (10–20%) sucrose-PBS solution and frozen for immunofluorescence or were fixed with 2% glutaraldehyde for transmission electron microscopy. Paraffin sections (2 μm) were processed for periodic acid-Schiff staining, periodic acid-silver methenamine staining, and immunostaining with specific primary antibodies, as shown in Table 1. Immunohistochemical staining was performed using standard procedures with an Avidin/Biotin Blocking Kit (Vector Laboratories, Burlingame, CA) and peroxidase-conjugated EnVision+Single Reagent (Dako, Glostrup, Denmark), and sections were visualized using diaminobenzidine (DAB substrate-chromogen system, Dako) or nitroblue tetrazolium (Roche Diagnostics, Mannheim, Germany) according to the manufacturers' instructions.

For immunofluorescence analysis, frozen sections and paraffin sections were used. Primary antibodies (β_1-integrin, synaptopodin, PAI-1, and CD31) were reacted with secondary antibodies labeled with Alexa 488 or 568 (Life Technologies, Carlsbad, CA) or rhodamine-conjugated secondary antibodies, respectively. Double immu-

Table 1. *Primary antibodies for immunostaining*

First Antibody	Application	Host Species	Dilution	Supplier
WT-1	IHC	Goat polyclonal antibody	1:200	Santa Cruz Biotechnology
PAI-1	IHC and IF	Rabbit polyclonal antibody	1:50 and 1:50	Santa Cruz Biotechnology
Synaptopodin	IF and IHC	Mouse monoclonal antibody	1:1 and 1:1	PROGEN Biotechnik
Fibrinogen	IHC	Rabbit polyclonal antibody	1:500	Dako Cytomation
uPAR	IE and IHC	Rat polyclonal antibody	1:30 and 1:50	R&D Systems
$\beta1$-Integrin	IF, WB, and IE	Rabbit polyclonal antibody	1:500 and 1:30	Novus Biologicals
α-Tublin	WB	Mouse monoclonal antibody	1:500	Sigma-Aldrich
CD31	IF	Rat polyclonal antibody	1:50	BD Pharmingen

IHC, immunohistochemistry; IF, immunofluorescence; IE, immunoelectronmicroscopy; WB, Western blot analysis.

nofluorescence was performed using standard procedures. Nuclear staining was performed using 4′,6-diamidino-2-phenylindole. For the quantitative determination of podocyte numbers, the WT-1-positive cells were counted in all glomeruli of each section on *days −1 and 8* (>30 glomeruli/mice), and at least 70 randomly selected glomeruli were counted on *day 12* under high-power magnification (×400). Average podocyte numbers per glomerulus were calculated on the basis of individual values. Thrombi and sclerosis were evaluated in periodic acid-silver methenamine-stained paraffin sections. Glomerular sclerosis and thrombosis scores were determined as follows. Each glomerulus was graded on a scale of *0–4*, representing the thrombotic or sclerotic area involving 0%, 1–25%, 26–50%, 51–75%, or >75% of the glomerulus, respectively. Glomeruli ($n > 70$) for each section were averaged and defined as the thrombosis score or sclerosis score per mouse, separately ($n = 6$).

RNA Extraction and Quantitative Real-Time PCR

Glomerular isolation was performed using ion powder perfusion and a magnet, as previously described (38). Total RNA was isolated using ISOGEN (Wako Pure Chemical Industries, Osaka, Japan). Total RNA was reverse transcribed using the Thermoscript RT-PCR System (Invitrogen, Karlsruhe, Germany) for first-strand cDNA. For quantitative analysis, all measured values were normalized to GAPDH gene expression using the $\Delta\Delta C_t$ method (C_t is threshold cycle), and results are presented as relative expression in arbitrary units. All primers used are shown in Table 2.

Western Blot Analysis

Samples were solubilized in RIPA buffer with protease inhibitors. Cytoplasmic proteins from cultured podocytes were extracted using a subcellular protein fractionation kit for cultured cells (Thermo Scientific, Pittsburgh, PA). Proteins were separated by 4–12% polyacrylamide gel electrophoresis (SDS-PAGE) and transferred to polyvinylidene difluoride membranes (PALL, Port Washington, NY). Blots were incubated with the primary antibodies shown in Table 1. After being washed in blocking solution, primary antibodies were detected using horseradish peroxidase-conjugated antibody (GE Healthcare, Buckinghamshire, UK) and a chemiluminescent substrate.

Cell Experiments

The immortalized mouse podocyte cell line (*passages 10–16*) used was a generous gift from Dr. Sakairi (Gunma University) (33). Cell differentiation was induced as previously described (39). All cell experiments were done under the following conditions and compared. Podocytes were treated in vitro with either uPA, PAI-1 alone, the PAI-1/uPA complex (PAI-1/uPA), or the PAI-1/uPA complex followed by anti-uPAR antibody (4 g/ml, R&D Systems, Minneapolis, MN) pretreatment (anti-uPAR + PAI-1/uPA). All compounds used were set by equimolar concentrations (5 nM). Glycosylated mouse PAI-1 (stable mutant) and active two-chain high-molecular-weight mouse uPA were purchased from Molecular Innovations (Novi, MI). The PAI-1/uPA complex was prepared by reacting 5 nM uPA with PAI-1 for 10 min at 37°C (40). After acid treatment for tight cell adhesion (5, 6), podocytes in individual wells were treated with uPA, PAI-1, the PAI-1/uPA complex, or anti-uPAR antibody before PAI-1/uPA complex administration. Anti-uPAR antibody was prepared by preincubation for 30 min at 37°C before the addition of the PAI-1/uPA complex.

Podocyte Detachment Assay

The podocyte detachment assay was analyzed by two blinded observers (M. Nagata and T. Ueno). Equal numbers of podocytes (4 × 10^3 cells/well) were seeded on 24-well plates precoated with collagen type I (0.03%) and treated under each condition described above.

Biotinylation of Cell Surface Protein Experiments

Surface biotinylation was performed using the Cell Surface Protein Isolation Kit (Pierce, Rockford, IL). Differentiated podocytes were biotinylated for 30 min at 4°C with 0.25 mg/ml sulfo-NHS-SS-biotin and then sonicated with lysis buffer. The biotinylated protein was extracted by an incubation with streptavidin-coupled beads for 60 min. After this, sample buffer containing DTT was added to the extraction buffer, and samples were incubated for 60 min using an end-over-end mixer followed by centrifugation. This procedure was performed for podocytes treated with uPA, PAI-1, the PAI-1/uPAR complex, or anti-uPAR + PAI-1/uPAR, and β_1-integrin expression was estimated by Western blot analysis.

Extraction of the Cytosolic Fraction

We used a subcellular protein fractionation kit for cultured cells (Thermo Scientific). Cells were detached by trypsin EDTA acid and

Table 2. *Sequence-specific primers for real-time PCR*

Gene	Sequence
Plasminogen activator inhibitor type 1	
Forward	5′-AGGATCGAGGTAAACGAGAGC-3′
Reverse	5′-GCGGGCTGAGATGACAAA-3′
Transforming growth factor-β	
Forward	5′-TGGAGCCTGGACACACAGTA-3′
Reverse	5′-TGTGTTGGTTGTAGAGGGCA-3′
Endothelial nitric oxide synthase	
Forward	5′-CCAGTGCCCTGCTTCATC-3′
Reverse	5′-GCAGGGCAAGTTAGGATCAG-3′
VEGF	
Forward	5′-CCAGCGAAGCTACTGCCGTCCA-3′
Reverse	5′-ACAGCGCATCAGCGGCACAC-3′
Desmin	
Forward	5′-GCGTGACAACCTGATAGACG-3′
Reverse	5′-GTTGGATTTCCTCCTGTAGTTTG-3′
Vimentin	
Forward	5′-GATCGATGTGGACGTTTCCAA-3′
Reverse	5′-ATACTGCTGGCGCACATCAC-3′

then centrifuged at 500 *g* for 5 min. After cells were washed, they were transferred to a microtube and pelleted by centrifugation at 500 *g* for 3 min. The cell pellet was obtained by discarding the supernatant. After this, cell extraction buffer with protease inhibitors was added and incubated with gentle mixing for 60 min at 4°C. The supernatant was immediately extracted as the cytoplasmic fraction after centrifugation at 500 *g* for 5 min.

Immunofluorescence in Cultured Podocytes

Podocytes grown on collagen type I-coated coverslips were treated under each condition described above and fixed with 4% paraformaldehyde in PBS. After being blocked with 50 mM glycine-PBS, podocytes were incubated with anti-uPAR antibody or anti-β_1-integrin antibody overnight followed by secondary antibodies conjugated with Alexa 488 (Life Technologies) or rhodamine for 2 h.

Double Immunogold Labeling of Ultrathin Cryosections

uPA- and PAI-1/uPA complex-treated cells were fixed in periodate lysine paraformaldehyde fixative for 6 h, pelleted, and then resuspended in 2.0% agarose (Wako Pure Chemical Industries, Osaka, Japan) as previously described (23). The grids were incubated on anti-β_1-integrin antibody and anti-uPAR antibody in 1% BSA overnight at 4°C followed by secondary antibodies of goat anti-rabbit 5-nm gold (BB, Cardiff, UK) or goat anti-rat 10-nm gold (BB) for 2 h at room temperature. Sections were stained with both uranyl acetate and lead citrate and inspected under a transmission electron microscope (model JEM-1400, JEOL, Tokyo, Japan) at 80 kV.

Statistics

Results are presented as means ± SE. Comparisons between two groups were performed using two-tailed Student's *t*-tests. Comparisons between three or more groups were performed using nonrepeated-measures ANOVA. *P* values of <0.05 were considered statistically significant. In the figures, *P* values are indicated as *$P < 0.05$, **$P < 0.01$, and ***$P < 0.001$.

RESULTS

Podocyte Depletion Caused Local Thrombotic Microangiopathy

NEP25/LMB2 mice developed significant proteinuria on *days 8* and *12* compared with control mice, and this was parallel with the decrease of WT-1 positive podocyte numbers, which was further diminished in glomeruli with thrombi compared with those without (Fig. 1, A–C). Serial section with fibrin immunostaining showed the association of local intracapillary thrombi with overlaying podocyte damage (Fig. 1, D and E). This was confirmed by double immunolabeling showing that segments lacking WT-1-positive cells were associated with fibrin in the corresponding capillary (Fig. 1F). Electron microscopy demonstrated that intracapillary coagulation debris and mesangiolysis were associated with degeneration or detachment of overlaying podocytes (Fig. 1G). These findings indicate that podocyte loss causes local thrombotic microangiopathy in this model.
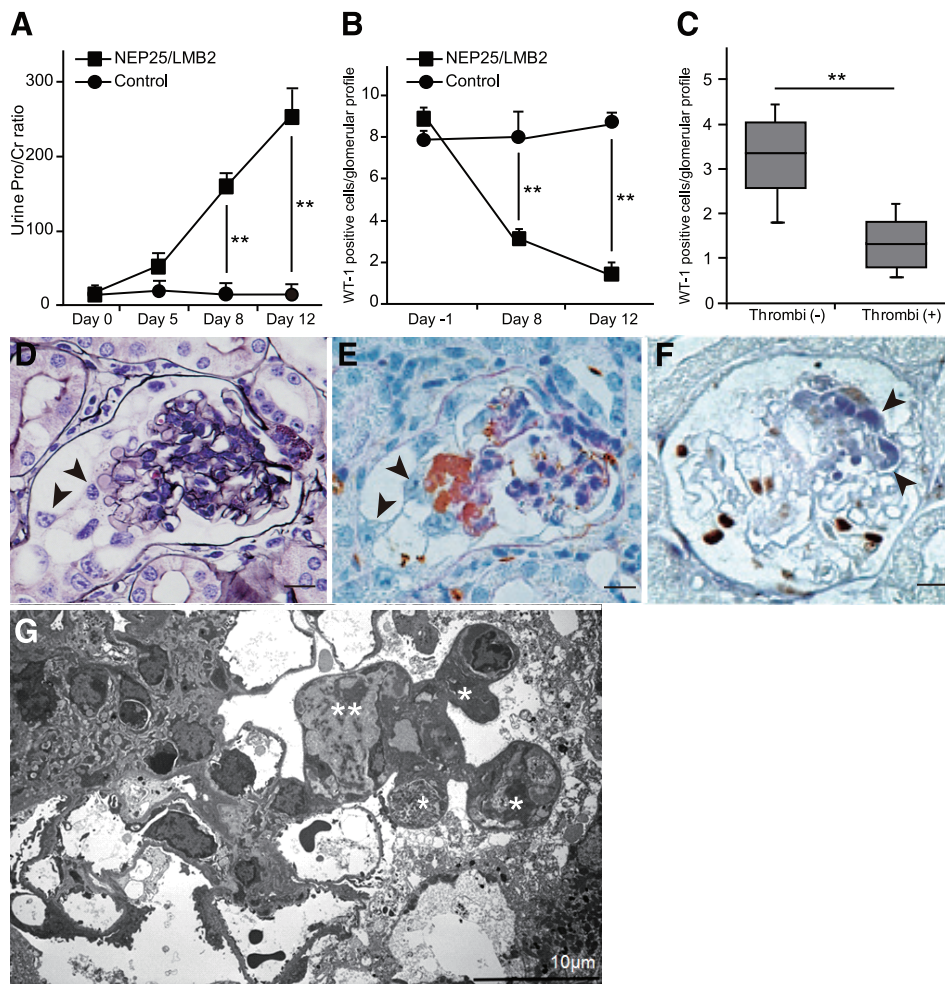

Fig. 1. Podocyte-specific injury evoked progressive proteinuria and microangiopathy. *A*: NEP25/LMB2 mice developed proteinuria on *day 5*, reaching significant levels on *days 8* and *12*, compared with control mice (*n* = 6 mice/group). Urinary Pro/Cr ratio, urinary protein-to-creatinine ratio. **$P < 0.01$. *B*: the number of Wilms tumor 1 (WT-1)-positive podocytes was significantly reduced in NEP25/LMB2 mice (*n* = 6) compared with control mice (*n* = 6). **$P < 0.01$. *C*: in NEP25/LMB2 mice, glomeruli without thrombi [Thrombi(−)] had significantly greater numbers of WT-1-positive cells compared with glomeruli with thrombi [Thrombi(+)] on *day 12*. Average numbers of glomeruli of glomeruli without and with thrombi were 27.1 ± 7.61 and 73.6 ± 11.4, respectively. **$P < 0.01$. *D*: representative glomerular features of NEP25/LMB2 mice on *day 12*. Thrombi were detected at the site of podocyte injury (arrowhead, periodic acid-silver methenamine). *E*: fibrinogen immunostaining on serial sections from *D* showing fibrinogen (brown) in the glomerular tuft with injured podocytes (arrowhead, counterstained with periodic acid-Schiff). *F*: double immunolabeling with fibrinogen (blue) and WT-1 (brown). Fibrinogen was found at the site where WT-1 disappeared (arrowhead). Original magnification: ×400. Scale bars = 15 μm in *D–F*. *G*: transmission electron microscopy (EM) of the glomerulus in NEP25/LMB2 mice on *day 12*. Intracapillary coagulation debris (*) and mesangiolysis (**) were associated with degeneration or detachment of overlaying podocytes. Original magnification: ×400. Scale bar = 10 μm.

Endothelial PAI-1 Upregulation as an Early Response to Podocyte Injury

In NEP25/LMB2 mice, glomerular mRNA of VEGF and endothelial nitric oxide synthase (eNOS) was decreased with the thrombosis score on *day 12* (Fig. 2, *A–C*). Transforming growth factor-β and PAI-1 transcripts were significantly elevated on *day 1* in NEP25/

LMB2 mice after LMB2 injection (Fig. 2, *D* and *E*). In NEP25/LMB2 mice on *day 1*, PAI-1 was expressed in a diffuse and global pattern and colocalized with the endothelial cell marker CD31 by double immunofluorescence, whereas PAI-1 was not expressed in control mice (Fig. 2F). At the later stage, on *day 12*, PAI-1 was expressed in preserved capillaries and podocytes (Fig. 2G). uPAR
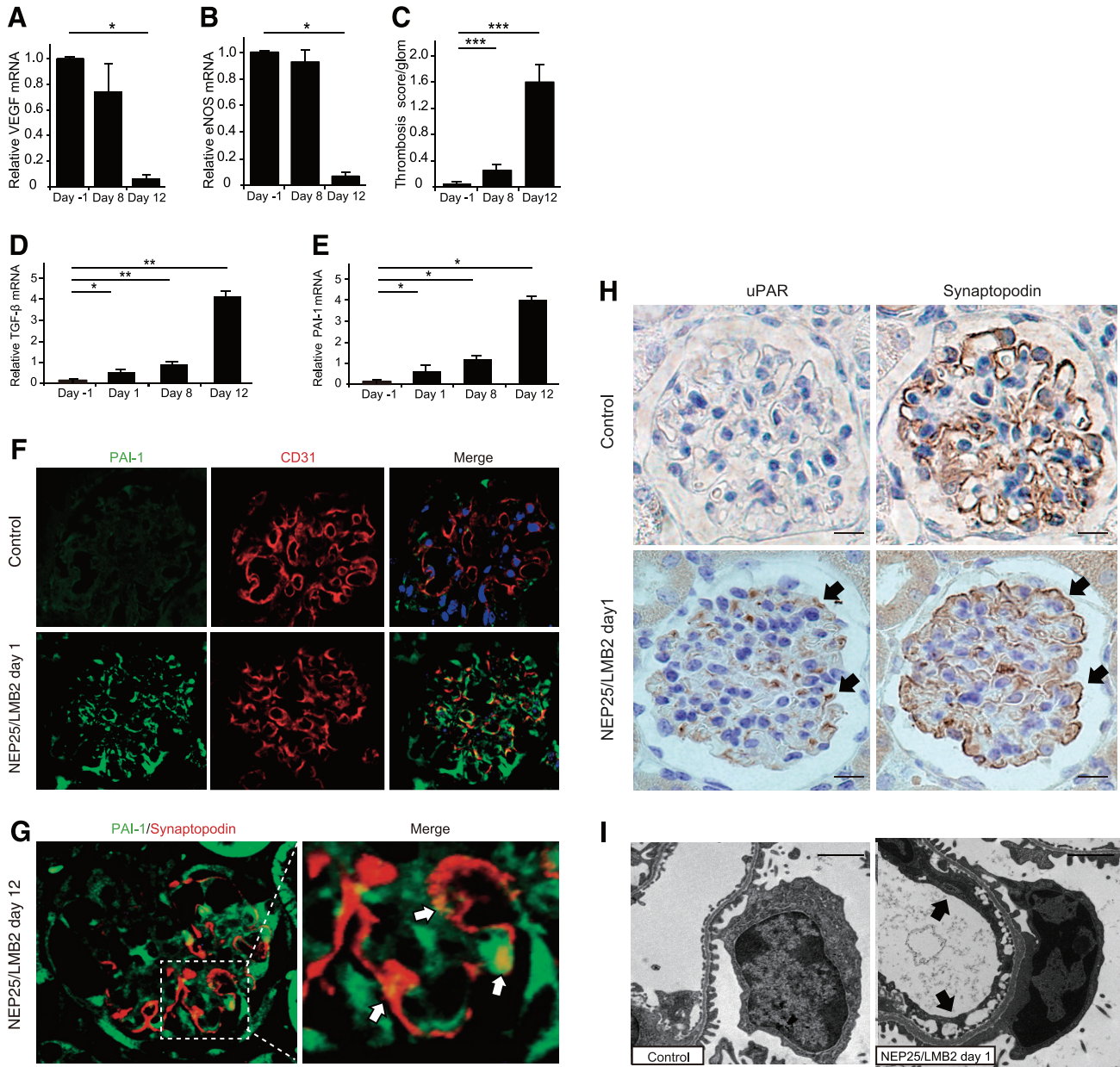
Fig. 2. Upregulation of plasminogen activator inhibitor type 1 (PAI-1) as an early endothelial response against podocyte injury. *A* and *B*: in NEP25/LMB2 mice, glomerular mRNA expression of the endothelial dysfunction markers VEGF and endothelial nitric oxide synthase (eNOS) was decreased on *day 12*. *$P < 0.05$. *C*: compared with *day −1*, the thrombosis score was significantly elevated on *day 12* in NEP25/LMB2 mice ($n = 6$). ***$P < 0.001$. *D* and *E*: transforming growth factor (TGF)-β mRNA expression in isolated glomeruli (*D*) and relative PAI-1 mRNA (*E*). TGF-β mRNA was increased in NEP25/LMB2 mice on *day 1* and further increased on *days 8* and *12*. PAI-1 mRNA expression in isolated glomeruli was increased on *day 1* and further increased on *days 8* and *12*. $n = 5$ mice/group for each time point. *$P < 0.05$; **$P < 0.01$. *F*: double immunofluorescence of PAI-1 and CD31 expression in control and NEP25/LMB2 mice in glomeruli on *day 1*. Magnification: ×600. PAI-1 was absent in control mice, whereas it was expressed and colocalized with CD31 in NEP25/LMB2 mice. *G*: on *day 12*, PAI-1 was aberrantly expressed in the podocyte cytoplasm in NEP25/LMB2 mice. *H*: expression of urokinase plasminogen activator (uPA) receptor (uPAR) in NEP25/LMB2 mice on *day 1* as revealed by serial sections. uPAR was not expressed in control mice (*top*), whereas it was expressed mainly in podocytes in NEP25/LMB2 mice (*bottom*), as confirmed in synaptopodin staining by serial sections (arrows). *I*: electron microscopy showed endothelial cell swelling and loss of fenestra (arrows) accompanied with overlaying podocyte foot process effacement in NEP25/LMB2 mice compared with control mice on *day 1*. Scale bars = 2 μm.

was expressed in podocytes in NEP25/LMB2 mice on *day 1* by serial section analysis, and it was absent in control mice (Fig. 2*H*). Electron microscopy showed the association of endothelial injury and overlaying podocyte damage in NEP25/LMB2 mice (Fig. 2*I*).

Inhibition of PAI-1 Ameliorated Microangiopathy and Protected Podocyte Loss

Treatment with the PAI-1 inhibitor TM5484 decreased glomerular PAI-1 expression in NEP25/LMB2 mice on *day 1* compared with vehicle-treated mice (Fig. 3*A*). TM5484 significantly ameliorated proteinuria and thrombosis and preserved podocyte numbers compared with NEP25/LMB2 + VH mice (Fig. 3, *B–D*). In addition, glomerular mRNA levels of eNOS and VEGF in NEP25/LMB2 + PI mice were higher and podocyte injury markers desmin and vimentin were lower than those in NEP25/LMB2 + VH mice

(Fig. 3*E*). Light and electron microscopy showed that glomerular structure and podocytes were preserved and glomerulosclerosis was significantly decreased in NEP25/LMB2 + PI mice on *day 12* (Fig. 4, *A* and *B*). Immunofluorescence microscopy revealed that β_1-integrin on the basal surface of podocytes did not colocalize with synaptopodin in control or NEP25/LMB2 + PI mice, whereas β_1-integrin was located in the cytoplasm of podocytes in NEP25/LMB2 + VH mice, indicating that PAI-1-mediated β_1-integrin translocation in NEP25/LMB2 mice was protected by PAI-1 inhibitor in vivo (Fig. 5).

Heparin Loading Interfered With Thrombi But Had No Effect on Podocyte Protection

Heparin loading experiments showed no effect on proteinuria and podocyte number despite the suppression of throm-
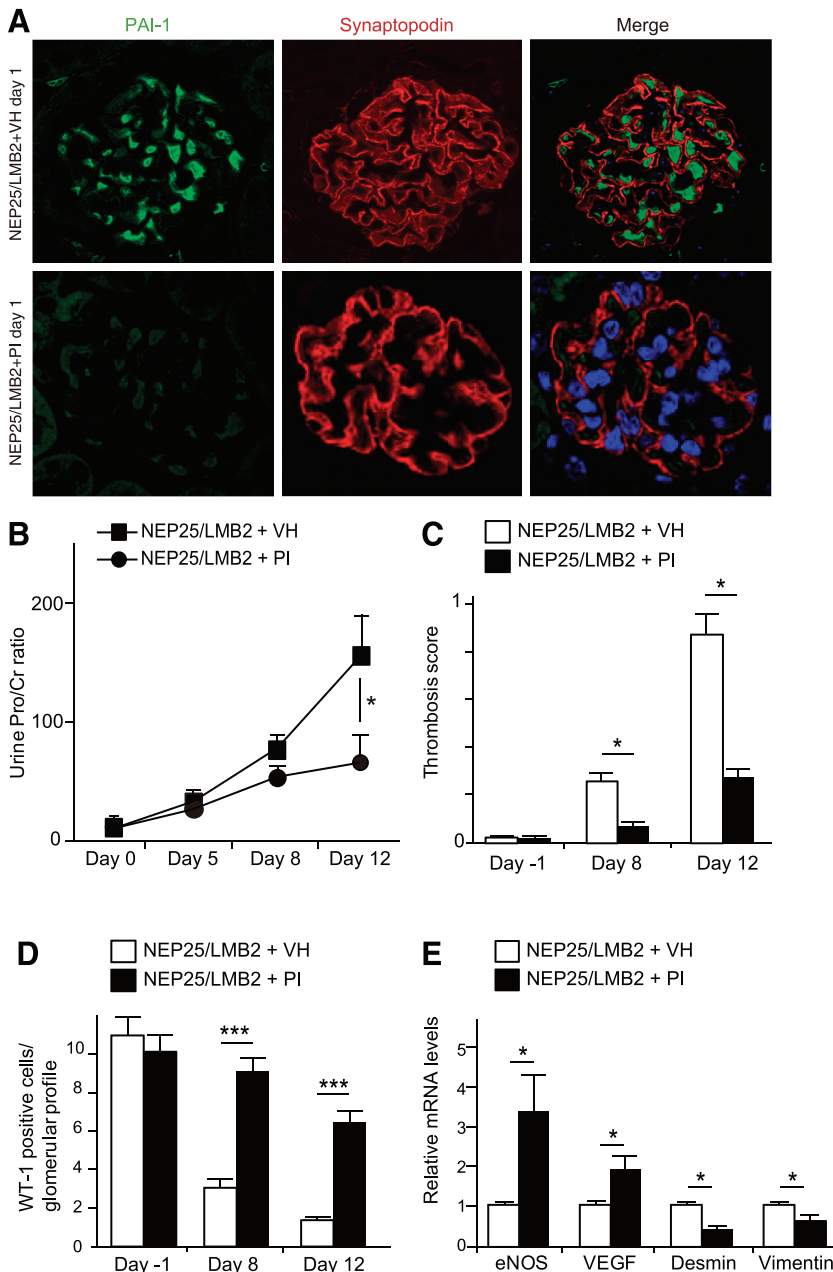

Fig. 3. PAI-1 inhibitor ameliorated proteinuria and preserved podocyte numbers in NEP25/LMB2 mice. *A*: expression of PAI-1 was reduced in PAI-1 inhibitor-treated NEP25/LMB2 mice (NEP25/LMB2 + PI group) compared with vehicle-treated NEP25/LMB2 mice (NEP25/LMB2 + VH group). *B*: proteinuria in NEP25/LMB2 + PI mice (*n* = 8) was significantly lower than that in NEP25/LMB2 + VH mice (*n* = 6) on *day 12*. *P < 0.05. *C*: the thrombosis score was significantly lower in NEP25/LMB2 + PI mice (*n* = 8) than in NEP25/LMB2 + VH mice (*n* = 6). *P < 0.05. *D*: mean WT-1-positive cells per glomerular profile in NEP25/LMB2 + PI mice (*n* = 8) were significantly higher than those in NEP25/LMB2 + VH mice (*n* = 6). ***P < 0.001. *E*: relative mRNA expression from isolated glomeruli on *day 12* in NEP25/LMB2 + PI mice (*n* = 5) and NEP25/LMB2 + VH mice (*n* = 5) was compared. Glomeruli were isolated from each mouse, and quantitative real-time PCR was done on each sample. NEP25/LMB2 + PI mice showed significantly higher levels in eNOS and VEGF mRNA but significantly lower levels of desmin and vimentin mRNA compared with NEP25/LMB2 + VH mice.
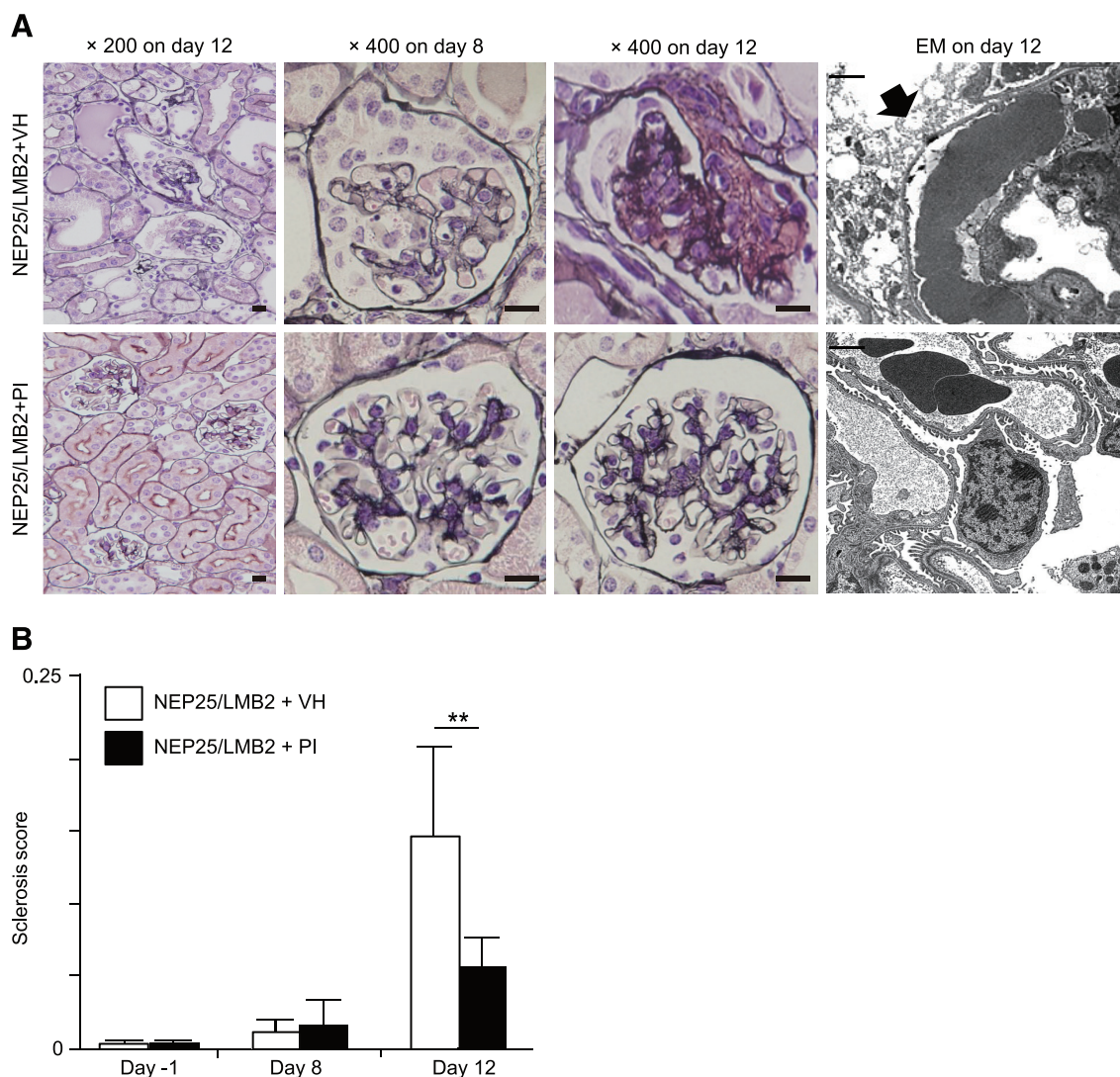
Fig. 4. PAI-1 inhibitor protected glomerular structure and podocyte injury in NEP25/LMB2 mice. *A*: histology of the kidney cortex. At lower magnification (×200; scale bars = 15 μm), NEP25/LMB2 + PI mice showed less glomerular injury and tubular dilatation than NEP25/LMB2 + VH mice (*left*). Higher magnification (×400, scale bars = 15 μm) of periodic acid-silver methenamine staining revealed glomerular epithelial proliferation and thrombi on *day 8* (*middle left*) and glomerulosclerosis on *day 12* (*middle right*) in NEP25/LMB2 + VH mice. Bowman's space cells were interpreted as proliferating parietal epithelial cells and may well represent podocytes undergoing detachment in NEP25/LMB2 + VH mice on *day 8*. Relatively normal glomeruli were noted in NEP25/LMB2 + PI mice. A transmission EM image of the glomerulus on *day 12* is shown on the *right*. In NEP25/LMB2 + VH mice, thrombotic formation was associated with degeneration in overlaying podocytes (arrow). These features were not observed, and the foot process was preserved in NEP25/LMB2 + PI mice. Scale bars = 2 μm. *B*: prevalence of glomerulosclerosis in NEP25/LMB2 mice with or without PAI-1 inhibitor. The sclerosis score was significantly lower in NEP25/LMB2 + PI mice ($n = 8$) than in NEP25/LMB2 + VH mice ($n = 6$). **$P < 0.01$.

botic formation, suggesting that thrombi per se do not act on podocyte loss (Fig. 6, *A–C*).

PAI-1/uPA Complex-Induced Podocyte Detachment In Vitro Required uPAR-Dependent β_1-Integrin Endocytosis

The mechanism underlying podocyte protection by the PAI-1 inhibitor in vivo was tested using established mouse podocytes in vitro. PAI-1/uPA-treated podocytes showed a significant cell detachment with a loss of arborized shape, whereas this was not seen in podocytes treated with uPA and PAI-1 alone. Apoptotic bodies and caspase-3-positive cells were not observed upon podocyte detachment (data not shown). In addition, podocytes treated with anti-uPAR antibody targeting the PAI-1/uPA complex (anti-uPAR + PAI-1/

uPA) did not exhibit podocyte detachment, indicating that PAI-1/uPA-mediated podocyte detachment was uPAR dependent (Fig. 7). Using confocal immunofluorescence microscopy, cultured podocytes treated with the PAI-1/uPA complex expressed β_1-integrin in the cytoplasm that colocalized with uPAR expression, despite the absence of such translocation in podocytes treated with uPA or PAI-1 alone or with anti-uPAR + PAI-1/uPA (Fig. 8, *A* and *B*). Biotinylated experiments showed a reduction of membrane β_1-integrin only in PAI-1/uPA-treated cells. Western blot analysis showed an increase of β_1-integrin in the cytoplasmic fraction of PAI-1/uPA-treated podocytes but not those with other treatments (Fig. 9, *A* and *B*). In addition, double immunogold labeling electron microscopy showed a disappearance of cell surface
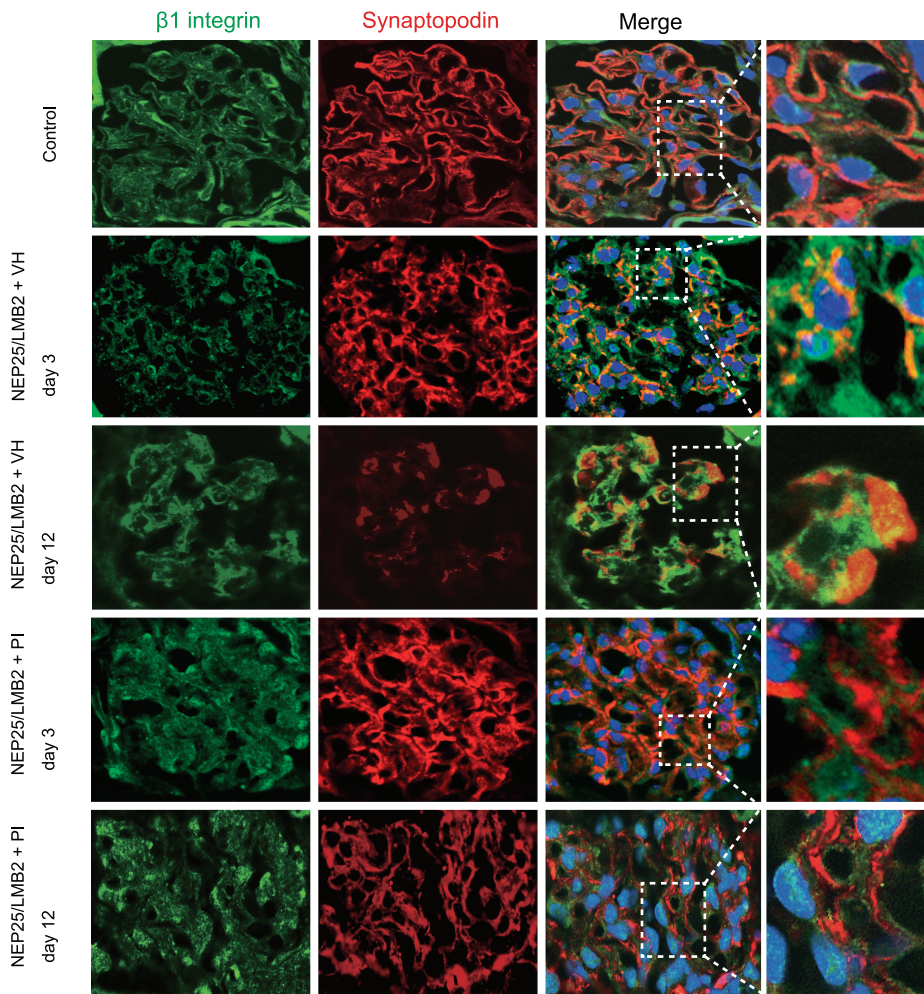
Fig. 5. β_1-Integrin was expressed in the cytoplasm of podocytes in NEP25/LMB2 mice. In control mice, β_1-integrin was detected in the mesangium and along the glomerular basement membrane (GBM) and did not overlap with synaptopodin. In NEP25/LMB2 + VH mice on *days 3* and *12*, β_1-integrin was found in the podocyte cytoplasm and occasionally colocalized with synaptopodin. Such β_1-integrin translocation was not apparent in NEP25/LMB2 + PI mice on *days 3* and *12*. Magnification: $\times 600$.

β_1-integrin and colocalization of β_1-integrin and uPAR within the endocytotic vesicles of PAI-1/uPA-treated podocytes (Fig. 9*C*). The cytoplasmic shift of β_1-integrin and uPAR was confirmed by counting gold particles (Fig. 9*D*).

DISCUSSION

The present study describes novel mechanism of podocyte loss by aberrant intracapillary signaling, which, in turn, targets podocytes by pathological PAI-1-mediated and uPAR-dependent β_1-integrin internalization, resulting cell detachment.

Our first observation was that induced podocyte-specific injury correlated with thrombosis in glomeruli. Double immunolabeling and electron microscopy displayed an association of focal thrombi with damage in overlying podocytes. Because our heparin loading experiments suppressed thrombi without changing podocyte number, thrombosis has no significant responsibility for podocyte loss. These findings support the notion that podocyte dysfunction causes glomerular TMA and suggests that podocyte-intracapillary signaling is locally regulated. Generally, TMA appeared in the setting of severe endothelial cell injury, such as hemolytic uremic syndrome, which seems to be mediated by PAI-1, a strong effector of antifibrinolysis (2, 31). Normally, PAI-1 is not produced in kidneys but is elevated in glomeruli in cases with crescentic glomerulonephritis, which accompanies fibrin exudation (20). This may

reflect severe glomerular endothelial cell injury and is thought to be a response to tissue fibrinolysis.

In our model of NEP25/LMB2 mice, expression of glomerular PAI-1 protein revealed some unique features, i.e., a diffuse pattern in a de novo fashion in glomerular endothelial cells as early as 1 day after LMB2 injection. Since LMB2 binds to human CD25 and mouse endothelial cells do not express it, glomerular PAI-1 upregulation 1 day after LMB2 injection is caused by LMB2-induced podocyte injury but not a direct action of LMB2 in glomerular endothelial cells (26).

Notably, this was before decreases in VEGF and eNOS mRNA expression as well as the formation of glomerular TMA lesions. The ultrastructure on *day 1* showed podocyte foot process effacement accompanied by endothelial cell swelling but not with platelet accumulation or thrombi in NEP25/LMB2 mice. Because LMB2 immediately binds to and injures podocytes, diffuse PAI-1 expression in endothelial cells on *day 1* suggests that PAI-1 synthesis is an early endothelial response to podocyte injury but may not be the same for antifibrinolytic actions. Of note, we also demonstrated de novo expression of uPAR in podocytes, not in endothelial cells, on *day 1*. Thus, podocyte injury rapidly activates aberrant endothelium-podocyte signaling in vivo. At the later stage where glomerular TMA was apparent, PAI-1 was also expressed in preserved capillaries but not in the portion of thrombi, implicating that
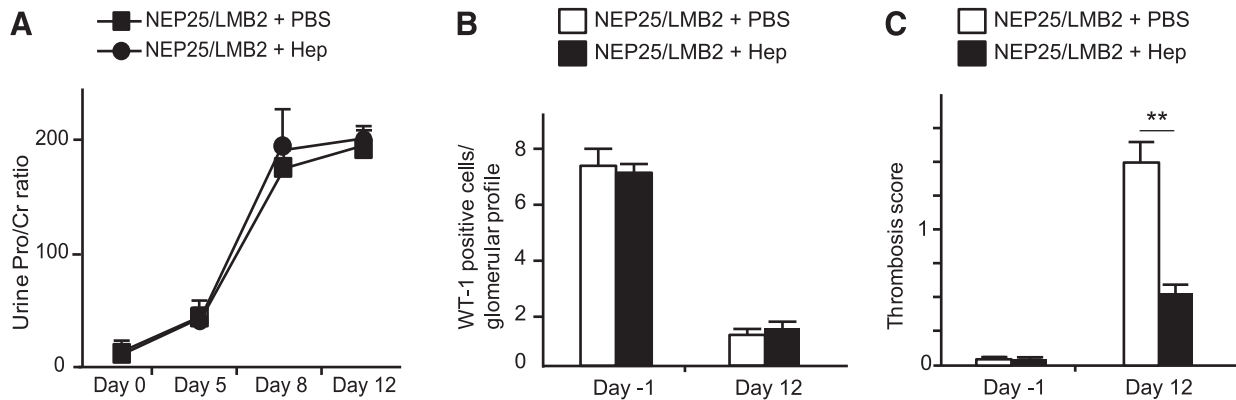
Fig. 6. Interference with thrombosis by heparin loading had no effect on proteinuria and podocyte numbers. *A*: proteinuria levels were similar in mice treated with (NEP25/LMB2 + Hep group; *n* = 5) or without heparin (NEP25/LMB2 + PBS group; *n* = 5). *B*: mean WT-1-positive cells per glomerular profile in NEP25/LMB2 + Hep mice (*n* = 5) were similar to those in NEP25/LMB2 + PBS mice (*n* = 5) on *days −1* and *12*. *C*: the thrombosis score in NEP25/LMB2 + Hep mice (*n* = 5) was significantly lower on *day 12* compared with that in NEP25/LMB2 + PBS mice (*n* = 5). **$P < 0.01$.

activated endothelial cells persistently expressed PAI-1. The absence of PAI-1 at thrombi may be due to the loss of endothelial cells, as shown in our electron microscopy experiments (Fig. 1*G*). Importantly, we showed colocalization of PAI-1 and synaptopodin in this late stage. Since uPAR, a receptor of PAI-1, was shown to be expressed in podocytes among several models of nephrosis (41), endothelium-derived
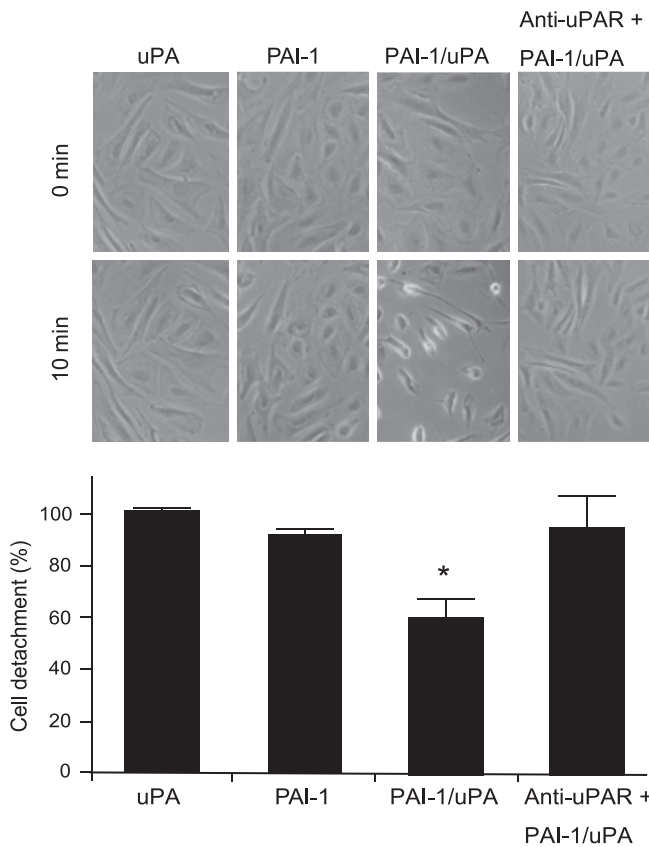

Fig. 7. PAI-1 and the uPA complex induced cell detachment in podocytes in vitro. We evaluated podocyte adhesive capabilities by manual counting cells. All experiments were repeated three times and statistically estimated. The number of podocytes incubated with the PAI-1/uPA complex was significantly reduced compared with those incubated with uPA, PAI-1 alone, and anti-uPAR + PAI-1/uPA. *$P < 0.05$ vs. uPA, PAI-1, and anti-uPAR + PAI-1/uPA.
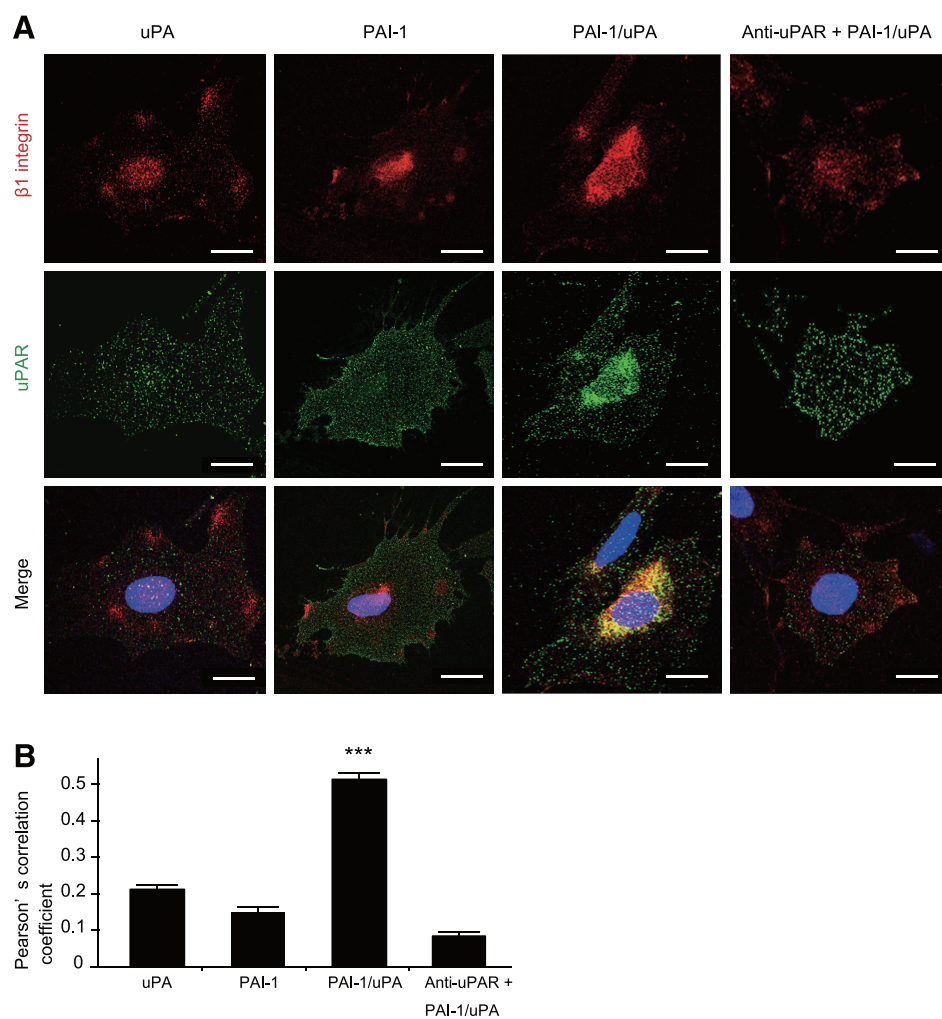
PAI-1 may pass through the GBM and form a complex with uPAR during podocyte injury.

PAI-1 is known to have pleiotropic functions, including effects on cell motility, activation of apoptosis, and promotion of cell senescence, some of which may contribute to the progression of glomerular damage (9, 11, 24, 35). Although several reports have shown glomerular PAI-1 expression in glomerular diseases (14, 29, 45), the role of PAI-1 in podocyte diseases has not been extensively explored. In this regard, the present study investigated the actions of PAI-1 during podocyte injury by several experiments. First, we administered a PAI-1 inhibitor immediately after LMB2 treatment and found suppression of thrombosis and maintained VEGF and eNOS levels in NEP25/LMB2 mice, suggestive of endothelial protection. Moreover, PAI-1 inhibitor treatment showed significantly less proteinuria and higher podocyte numbers in NEP25/LMB2 mice compared with vehicle-treated NEP25/LMB2 mice. This suggests that intracapillary PAI-1 impacted the glomerular filtration barrier and particularly promoted podocyte loss. Second, because it is unknown whether the effect of PAI-1 inhibitor on podocyte protection was by direct or indirect actions through fibrinolysis, we performed heparin loading experiments in our model. Heparin loading significantly reduced thrombosis but had no effects on proteinuria and podocyte number. These observations may provide a novel action of PAI-1, other than fibrinolysis, as an aberrant intracapillary podocyte danger signal during podocyte injury.

Our hypothesis that primary podocyte injury causes secondary podocyte loss by the above-described PAI-1 mechanism suggests a positive feedback loop of podocyte loss. Using podocyte-specific CD25 chimeric mice, Matsusaka et al. (25) showed that LMB2 induced primary podocyte injury in CD25-positive podocytes only, even though neighboring podocytes lacking CD25 were secondarily damaged. This observation provides important clues to understanding progressive glomerulosclerosis promoted by a vicious cycle of podocyte loss as a "domino effect," and our hypothesis of an intracapillary danger signal toward podocytes may explain this phenomenon.

Our additional experiments in vitro disclosed the mechanism whereby intracapillary PAI-1 upregulation triggered secondary to podocyte loss. Basically, motility of cells requires the proper function of cytoskeletal and cell membrane dynamics (4). It is

Fig. 8. The PAI-1/uPA complex induced translocation of β_1-integrin from the podocyte surface to the cytoplasm via a uPAR-dependent mechanism. *A*: localization of β_1-integrin and uPAR was visualized by confocal laser scanning microscopy. Using immunofluorescence microcopy, cultured podocytes treated with the PAI-1/uPA complex expressed β_1-integrin in the cytoplasm that colocalized with uPAR, whereas no translocalization occurred in podocytes treated with uPA or PAI-1 alone. β_1-Integrin translocalization in response to PAI-1/uPA could be inhibited by the administration of anti-uPAR. Magnification: $\times 1,000$. Scale bars = 10 μm. *B*: colocalization between β_1-integrin and uPAR was significantly augmented in PAI-1/uPA-treated cells ($n = 30$ cells/group). ***$P < 0.001$ vs. uPA, PAI-1, and anti-uPAR + PAI-1/uPA. Pearson's correlation coefficient for β_1-integrin and uPAR colocalization was calculated using ImageJ and JaCoP software (3, 34). In every experiment using JaCoP software, the red fluorescence indirectly emitted by β_1-integrin was primarily detected in Ch1 and the green fluorescence indirectly emitted by uPAR was primarily detected in Ch2. In all calculations, the background was subtracted from the intensity values.

known that tissue PAI-1 acts to promote cell motility and proliferation by the uPA/uPAR complex, one of the mechanisms of cancer metastasis (5, 6, 37). Integrins are key molecules maintaining cell integrity via matrix-cytoskeleton signaling as transmembrane receptors (4).

In the podocyte, $\alpha_3\beta_1$-integrin is the main contributor of tight adhesion of podocytes to the GBM (32). Podocyte-specific β_1-integrin$^{flox/flox}$ mice exhibit foot process effacement, podocyte loss, and glomerulosclerosis (30). Czekay et al. (5, 6) showed that PAI-1/uPA complex-bound uPAR on the cell membrane promoted endocytosis of $\alpha_v\beta_3$-, $\alpha_v\beta_5$-, and $\alpha_3\beta_1$-integrins. In the present study, NEP25/LMB2 mice showed β_1-integrin in the podocyte cytoplasm on *day 12*, which was not observed in control mice, and was blocked by PAI-1 inhibitor. Additionally, immortalized podocytes treated with the PAI-1/uPA complex underwent significant cell detachment. Confocal immunofluorescence microscopy showed β_1-integrin and uPAR internalization only in PAI-1/uPA-treated podocytes. PAI-1/uPAR-mediated β_1-integrin internalization was confirmed by decreased membrane-localized β_1-integrin by biotinylated experiments and an increase of β_1-integrin protein in the cytoplasmic fraction. Furthermore, the double immunogold labeling technique displayed colocalization of β_1-integrin and uPAR within endocytotic vesicles after PAI-1/uPA treatment, suggesting endocytosis as a mechanism of β_1-integrin internalization.

In patients with FSGS, soluble uPAR is elevated in the serum and on the surface of podocytes. Wei et al. (41, 42) recently reported that uPAR-activated podocyte $\alpha_v\beta_3$-integrin resulted in the effacement of foot processes through disruption of the actin cytoskeleton. This mechanism could prime podocyte for detachment and then could be followed by endothelial PAI-1 induction, setting a progressive mechanism into motion. Clearly, more experiments are needed to link (soluble) uPAR-mediated podocyte injury and PAI-1-uPAR-β_1-integrin internalization, even though it is known that repression of β_1-integrin activates β_3-integrin via Rac1 and ERK (15). These observations, together with our present findings, suggest that primary podocyte injury accelerates progressive podocyte loss by upregulation of endothelial PAI-1-mediated podocyte β_1-integrin endocytosis. uPAR may have an important role in orchestrating disruption of integrin homeostatic functions to accelerate the cascade of responses leading to podocyte loss. The present study not only describes a novel mechanism of podocyte loss but also suggests that the PAI-1 inhibitor may be a possible therapeutic option for podocyte protection through the stabilization of β_1-integrin, similar to the suggested role for the B7-1 inhibitor abatacept (46). These
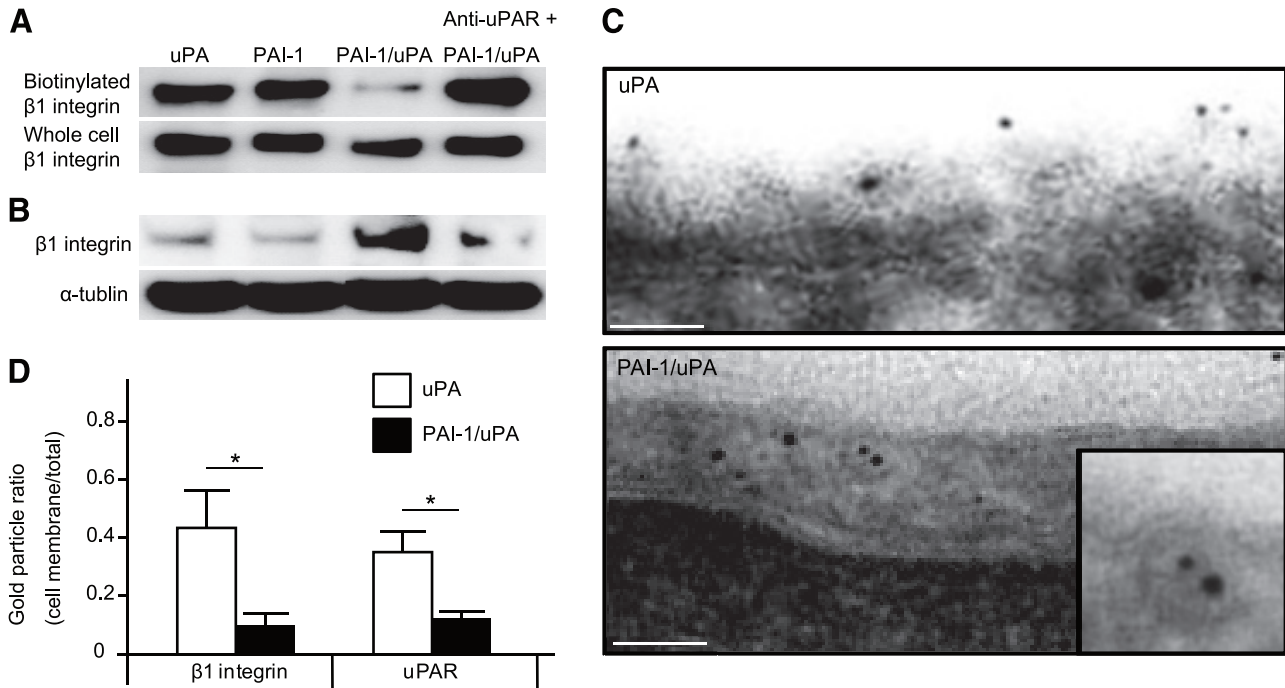
Fig. 9. The PAI-1/uPA complex induced β_1-integrin and uPAR translocation via an endosomal pathway. *A*: biotinylated experiments with Western blot analysis of β_1-integrin expression revealed a decrease of biotinylated membrane β_1-integrin in PAI-1/uPAR complex-treated podocytes. Such changes were not observed in podocytes treated with uPA, PAI-1 alone, or the anti-uPAR + PAI-1/uPA complex. *B*: β_1-integrin was increased in the cytoplasmic fraction in PAI-1/uPAR-treated podocytes. *C*: double immunogold labeling by immunoelectron microscopy of β_1-integrin (5-nm gold particles) and uPAR (10-nm gold particles). For uPA, both β_1-integrin and uPAR were predominantly located on the cell surface, whereas PAI-1/uPA showed colocalization of both proteins in the cytoplasm. Note that gold particles of both sizes were associated with endocytotic vesicles (*inset*). Scale bars = 50 nm. *D*: under ×40,000 magnification, gold particles of both sizes were counted, and the particle ratio in the cell membrane and total numbers of particles were calculated. Ratios of β_1-integrin and uPAR were significantly reduced in podocytes treated with PAI-1/uPA ($n = 6$) than in those treated with uPA ($n = 4$). *$P < 0.05$.

findings shed light into the new therapeutic strategies targeting podocyte integrin signaling.

In conclusion, primary podocyte injury stimulates upregulation of endothelial PAI-1, with the uPA/uPAR complex on the podocyte surface, resulting in podocyte detachment secondary to β_1-integrin endocytosis (Fig. 10). This mechanism may explain a vicious cycle of podocyte injury. Therefore, we suggest PAI-1 inhibition as a possible therapeutic option for the progression of glomerular injury inhibiting the vicious podocyte domino effect.
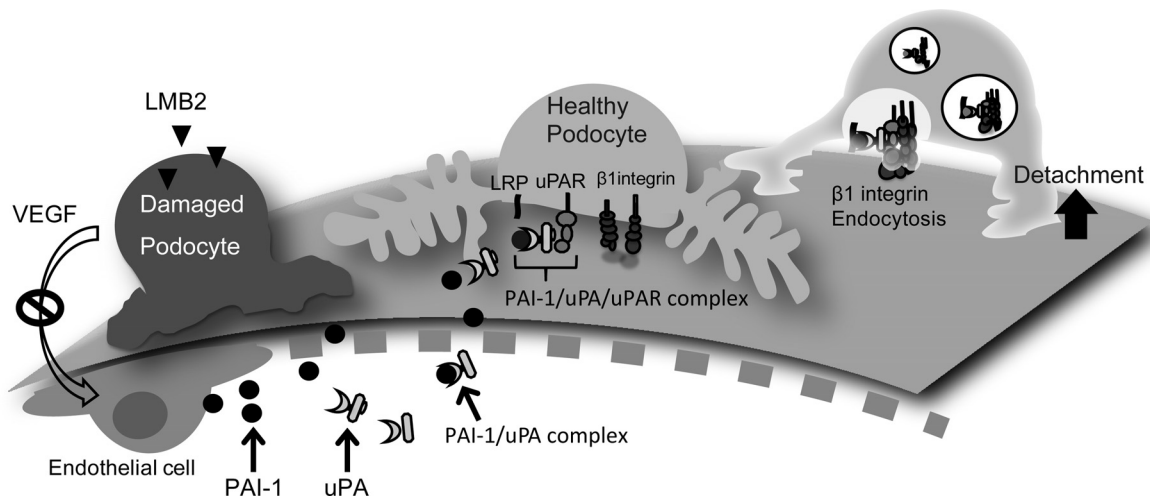

Fig. 10. Schematic demonstration of the podocyte domino effect by PAI-1/uPAR-mediated β_1-integrin endocytosis. From the *left*, damaged podocytes repressed VEGF expression, leading to endothelial dysfunction. Damaged endothelial cells produced and secreted PAI-1 (molecular mass: 45 kDa), which binds to circulating uPA (molecular mass: 31.5 kDa) either in the capillary or on the podocyte surface and then makes a complex with uPAR on the podocyte surface. The complex formation is able to bind β_1-integrin, which is known as a strong assembler of podocyte-GBM attachment. With the aid of a large endocytotic receptor, LDL receptor-related protein (LRP), on the podocyte surface (the expression of LRP was detected in vivo and cultured podocytes by real-time PCR in our preliminary experiments), β_1-integrin is translocated to the podocyte cytoplasm by endocytosis with the PAI-1/uPA/uPAR complex. Finally, β_1-integrin-lost primary healthy podocytes undergo detachment from the GBM.

REFERENCES

1. **Aita K, Etoh M, Hamada Yokoyama C H, Takahashi A, Suzuki T, Hara M, Nagata M.** Acute and transient podocyte loss and proteinuria in preeclampsia. *Nephron Clin Pract* 112: c65–c70, 2009.
2. **Bergstein JM, Riley M, Bang NU.** Role of plasminogen-activator inhibitor type 1 in the pathogenesis and outcome of the hemolytic uremic syndrome. *N Engl J Med* 327: 755–759, 1992.
3. **Bolte S, Cordelières FP.** A guided tour into subcellular colocalization analysis in light microscopy. *J Microsc* 224: 213–232, 2006.
4. **Brooks PC, Klemke RL, Schon S, Lewis JM, Schwartz MA, Cheresh DA.** Insulin-like growth factor receptor cooperates with integrin alpha v beta 5 to promote tumor cell dissemination in vivo. *J Clin Invest* 99: 1390–1398, 1997.
5. **Czekay RP, Aertgeerts K, Curriden SA, Loskutoff DJ.** Plasminogen activator inhibitor-1 detaches cells from extracellular matrices by inactivating integrins. *J Cell Biol* 160: 781–791, 2003.
6. **Czekay RP, Loskutoff DJ.** Plasminogen activator inhibitors regulate cell adhesion through a uPAR-dependent mechanism. *J Cell Physiol* 220: 655–663, 2009.
7. **D'Agati VD.** Podocyte injury in focal segmental glomerulosclerosis: lessons from animal models (a play in five acts). *Kidney Int* 73: 399–406, 2008.
8. **D'Agati VD, Kaskel FJ, Falk RJ.** Focal segmental glomerulosclerosis. *N Engl J Med* 365: 2398–2411, 2011.
9. **Dellas C, Loskutoff DJ.** Historical analysis of PAI-1 from its discovery to its potential role in cell motility and disease. *Thromb Haemost* 93: 631–640, 2005.
10. **Eddy AA, Fogo AB.** Plasminogen activator inhibitor-1 in chronic kidney disease: evidence and mechanisms of action. *J Am Soc Nephrol* 17: 2999–3012, 2006.
11. **Elzi DJ, Lai Y, Song M, Hakala K, Weintraub ST, Shiio Y.** Plasminogen activator inhibitor 1-insulin-like growth factor binding protein 3 cascade regulates stress-induced senescence. *Proc Natl Acad Sci USA* 109: 12052–12057, 2012.
12. **Eremina V, Jefferson JA, Kowalewska J, Hochster H, Haas M, Weisstuch J, Richardson C, Kopp JB, Kabir MG, Backx PH, Gerber HP, Ferrara N, Barisoni L, Alpers CE, Quaggin SE.** VEGF inhibition and renal thrombotic microangiopathy. *N Engl J Med* 358: 1129–1136, 2008.
13. **George M, Rainey MA, Naramura M, Foster KW, Holzapfel MS, Willoughby LL, Ying G, Goswami RM, Gurumurthy CB, Band V, Satchell SC, Band H.** Renal thrombotic microangiopathy in mice with combined deletion of endocytic recycling regulators EHD3 and EHD4. *PLos One* 6: e17838, 2011.
14. **Hamano K, Iwano M, Akai Y, Sato H, Kubo A, Nishitani Y, Uyama H, Yoshida Y, Miyazaki M, Shiiki H, Kohno S, Dohi K.** Expression of glomerular plasminogen activator inhibitor type I in glomerulonephritis. *Am J Kidney Dis* 39: 695–705, 2002.
15. **Hayashida T, Jones JC, Lee CK, Schnaper HW.** Loss of β1-integrin enhances TGF-β1-induced collagen expression in epithelial cells via increased αvβ3-integrin and Rac1 activity. *J Biol Chem* 285: 30741–30751, 2010.
16. **Hedberg A, Fismen S, Fenton KA, Fenton C, Osterud B, Mortensen ES, Rekvig OP.** Heparin exerts a dual effect on murine lupus nephritis by enhancing enzymatic chromatin degradation and preventing chromatin binding in glomerular membranes. *Arthritis Rheum* 63: 1065–1075, 2011.
17. **Ichimura A, Matsumoto S, Suzuki S, Dan T, Yamaki S, Sato Y, Kiyomoto H, Ishii N, Okada K, Matsuo O, Hou FF, Vaughan DE, van Ypersele de Strihou C, Miyata T.** A small molecule inhibitor to plasminogen activator inhibitor 1 inhibits macrophage migration. *Arterioscler Thromb Vasc Biol* 33: 935–942, 2013.
18. **Izuhara Y, Takahashi S, Nangaku M, Takizawa S, Ishida H, Kurokawa K, van Ypersele de Strihou C, Hirayama N, Miyata T.** Inhibition of plasminogen activator inhibitor-1: its mechanism and effectiveness on coagulation and fibrosis. *Arterioscler Thromb Vasc Biol* 28: 672–677, 2008.
19. **Izuhara Y, Yamaoka N, Kodama H, Dan T, Takizawa S, Hirayama N, Meguro K, van Ypersele de Strihou C, Miyata T.** A novel inhibitor of plasminogen activator inhibitor-1 provides antithrombotic benefits devoid of bleeding effect in nonhuman primates. *J Cereb Blood Flow Metab* 30: 904–912, 2010.
20. **Kitching AR, Kong YZ, Huang XR, Davenport P, Edgtton KL, Carmeliet P, Holdsworth SR, Tipping PG.** Plasminogen activator inhibitor-1 is a significant determinant of renal injury in experimental crescentic glomerulonephritis. *J Am Soc Nephrol* 14: 1487–1495, 2003.
21. **Kriz W, Gretz N, Lemley KV.** Progression of glomerular diseases: is the podocyte the culprit? *Kidney Int* 54: 687–697, 1998.
22. **Kriz W, Shirato I, Nagata M, LeHir M, Lemley KV.** The podocyte's response to stress: the enigma of foot process effacement. *Am J Physiol Renal Physiol* 304: F333–F347, 2013.
23. **Kurihara H, Harita Y, Ichimura K, Hattori S, Sakai T.** SIRP-α-CD47 system functions as an intercellular signal in the renal glomerulus. *Am J Physiol Renal Physiol* 299: F517–F527, 2010.
24. **Lijnen HR.** Pleiotropic functions of plasminogen activator inhibitor-1. *J Thromb Haemost* 3: 35–45, 2005.
25. **Matsusaka T, Sandgren E, Shintani A, Kon V, Pastan I, Fogo AB, Ichikawa I.** Podocyte injury damages other podocytes. Podocyte injury damages other podocytes. *J Am Soc Nephrol* 22: 1275–1285, 2011.
26. **Matsusaka T, Xin J, Niwa S, Kobayashi K, Akatsuka A, Hashizume H, Wang QC, Pastan I, Fogo AB, Ichikawa I.** Genetic engineering of glomerular sclerosis in the mouse via control of onset and severity of podocyte-specific injury. *J Am Soc Nephrol* 16: 1013–1023, 2005.
27. **Nagata M, Kriz W.** Glomerular damage after uninephrectomy in young rats. II. Mechanical stress on podocytes as a pathway to sclerosis. *Kidney Int* 42: 148–160, 1992.
28. **Nagata M.** Pathogenesis of glomerulosclerosis: role of epithelial interactions. *Clin Exp Nephrol* 4: 173–181, 2000.
29. **Nakamura T, Tanaka N, Hoguma N, Kazama T, Kobayashi I, Yokota S.** The localization of plasminogen activator inhibitor-1 in glomerular subepithelial deposits in membranous nephropathy. *J Am Soc Nephrol* 11: 2434–2444, 1996.
30. **Pozzi A, Jarad G, Moeckel GW, Coffa S, Zhang X, Gewin L, Eremina V, Hudson BG, Borza DB, Harris RC, Holzman LB, Phillips CL, Fassler R, Quaggin SE, Miner JH, Zent R.** β1 integrin expression by podocytes is required to maintain glomerular structural integrity. *Dev Biol* 316: 288–301, 2008.
31. **Rau JC, Beaulieu LM, Huntington JA, Church FC.** Serpins in thrombosis, hemostasis and fibrinolysis. *J Thromb Haemost* 5: 102–115, 2007.
32. **Sachs N, Sonnenberg A.** Cell-matrix adhesion of podocytes in physiology and disease. *Nat Rev Nephrol* 9: 200–210, 2013.
33. **Sakairi T, Abe Y, Jat PS, Kopp JB.** Cell-cell contact regulates gene expression in CDK4-transformed mouse podocytes. *Am J Physiol Renal Physiol* 299: F802–F809, 2010.
34. **Schneider CA, Rasband WS, Eliceiri KW.** NIH Image to ImageJ: 25 years of image analysis. *Nat Methods* 9: 671–675, 2012.
35. **Schneider DJ, Chen Y, Sobel BE.** The effect of plasminogen activator inhibitor type 1 on apoptosis. *Thromb Haemost* 100: 1037–1040, 2008.

36. **Slater SC, Ramnath RD, Uttridge K, Saleem MA, Cahill PA, Mathieson PW, Welsh GI, Satchell SC.** Chronic exposure to laminar shear stress induces Kruppel-like factor 2 in glomerular endothelial cells and modulates interactions with co-cultured podocytes. *Int J Biochem Cell Biol* 44: 1482–1490, 2012.

37. **Smith HW, Marshall CJ.** Regulation of cell signalling by uPAR. *Nat Rev Mol Cell Biol* 11: 23–36, 2010.

38. **Takemoto M, Asker N, Gerhardt H, Lundkvist A, Johansson BR, Saito Y, Betsholtz C.** A new method for large scale isolation of kidney glomeruli from mice. *Am J Pathol* 161: 799–805, 2002.

39. **Ueno T, Kobayashi N, Nakayama M, Takashima Y, Ohse T, Pastan I, Pippin JW, Shankland SJ, Uesugi N, Matsusaka T, Nagata M.** Aberrant Notch1-dependent effects on glomerular parietal epithelial cells promotes collapsing focal segmental glomerulosclerosis with progressive podocyte loss. *Kidney Int* 83: 1065–1075, 2013.

40. **Webb DJ, Thomas KS, Gonias SL.** Plasminogen activator inhibitor 1 functions as a urokinase response modifier at the level of cell signalling and thereby promotes MCF-7 cell growth. *J Cell Biol* 152: 741–752, 2001.

41. **Wei C, Möller CC, Altintas MM, Li J, Schwarz K, Zacchigna S, Xie L, Henger A, Schmid H, Rastaldi MP, Cowan P, Kretzler M, Parrilla R, Bendayan M, Gupta V, Nikolic B, Kalluri R, Carmeliet P, Mundel P, Reiser J.** Modification of kidney barrier function by the urokinase receptor. *Nat Med* 17: 55–63, 2008.

42. **Wei C, El Hindi S, Li J, Fornoni A, Goes N, Sageshima J, Maiguel D, Karumanchi SA, Yap HK, Saleem M, Zhang Q, Nikolic B, Chaudhuri A, Daftarian P, Salido E, Torres A, Salifu M, Sarwal MM, Schaefer F, Morath C, Schwenger V, Zeier M, Gupta V, Roth D, Rastaldi MP, Burke G, Ruiz P, Reiser J.** Circulating urokinase receptor as a cause of focal segmental glomerulosclerosis. *Nat Med* 17: 952–960, 2011.

43. **Wharram BL, Goyal M, Wiggins JE, Sanden SK, Hussain S, Filipiak WE, Saunders TL, Dysko RC, Kohno K, Holzman LB, Wiggins RC.** Podocyte depletion causes glomerulosclerosis: diphtheria toxin-induced podocyte depletion in rats expressing human diphtheria toxin receptor transgene. *J Am Soc Nephrol* 16: 2941–2952, 2005.

44. **Xu Y, Hagege J, Mougenot B, Sraer JD, Rønne E, Rondeau E.** Different expression of the plasminogen activation system in renal thrombotic microangiopathy and the normal human kidney. *Kidney Int* 50: 2011–2019, 1996.

45. **Yoshida Y, Shiiki H, Iwano M, Uyama H, Hamano K, Nishino T, Dohi K.** Enhanced expression of plasminogen activator inhibitor 1 in patients with nephrotic syndrome. *Nephron* 88: 24–29, 2001.

46. **Yu CC, Fornoni A, Weins A, Hakroush S, Maiguel D, Sageshima J, Chen L, Ciancio G, Faridi MH, Behr D, Campbell KN, Chang JM, Chen HC, Oh J, Faul C, Arnaout MA, Fiorina P, Gupta V, Greka A, Burke 3rd GW, Mundel P.** Abatacept in B7-1-positive proteinuric kidney disease. *N Engl J Med* 369: 2416–2423, 2013.